Tiron-loaded silver nanoparticles: Synthesis, physico-chemical and biological characterization for pharmacologically apt properties

Pratima Dutta
Guru Ghasidas University
Satendra Kumar Nirala
satendrak75@rediffmail.com

Guru Ghasidas University
Pavitra Behra
Guru Ghasidas University
Asim Amitabh Sahu
Guru Ghasidas University
Ankita Mukherjee
Guru Ghasidas University
Monika Bhadauria
Guru Ghasidas University

Research Article

Keywords: Nanotechnology, silver nanoparticles, tiron, cytotoxicity, genotoxicity

Posted Date: September 16th, 2025

DOI: https://doi.org/10.21203/rs.3.rs-7479494/v1

Additional Declarations: No competing interests reported.

Version of Record: A version of this preprint was published at BioNanoScience on December 17th, 2025. See the published version at https://doi.org/10.1007/s12668-025-02253-2.

Abstract

Nanotechnology offered synthesis of nanoparticles by unique combination of metals with natural and synthetic products for therapeutic uses with improved drug delivery. We synthesized tiron-loaded silver nanoparticles (TAgNPs), and performed their physico-chemical and biological characterization to understand pharmacologically apt properties. Synthesis of TAgNPs was confirmed by change in color to golden yellow with peak range of 430–440 nm under UV-visible spectroscopy. The particle size was found in the range of 14.9-12143.7 nm with a spherical shape under electron microscopy. Crystalline phase of tiron-loaded silver nanoparticles was observed by X-ray powder diffraction and thermal stability was confirmed by thermogravimetric analysis. Functional groups were validated under FTIR spectroscopy, which quantified functional groups on the surfaces of TAgNPs. The ability of TAgNPs to scavenge free radicals was evaluated with H_2O_2, DPPH and ABTS assays, which suggested its excellent antioxidant potential. *In vitro* cytotoxicity through MTT assay and genotoxicity through comet assay on rat lymphocytes suggested outstanding safety profile of TAgNPs. Thus, TAgNPs have pharmacologically apt physico-chemical and biological properties and may offer as a promising agent for medicinal use against toxic manifestations in terms of oxidative stress associated disorders.

1. Introduction

Nanoscience defines the atomic structures and molecules ranging between 1 and 100 nm or more, whereas nanomedicine established the foundation of nanoscience by improving drug delivery, diagnosis and treating diseases [1]. Nanotechnology involves size, shape, surface, electrical, thermal, and magnetic properties, which on integration with nanobiotechnology, plays important roles in drug delivery, disease diagnosis and its treatments [2]. Researchers developed nano-medicines like liposomes, dendrimers, nanotubes etcetera for targeted drug delivery in afflicted sites in the body [3]. Drugs embedded in the nano-carriers established several advantages, including increased solubility and bioavailability of drugs, targeted site delivery, raised stability of drug due to their smaller size and wider surface area [4]. Antimicrobial [5], antibacterial [5], antiviral [5], anticoagulant [5], anticancer [6], wound-healing [7], antifungal [8], antidiabetic [9], and anti-inflammatory properties [9] of various materials have been transformed into various nanoparticles for better efficacy and drug delivery.

Chelating agents effectively bind and eliminate toxic metals from the body [10]. Deferoxamine chelates free iron and aluminum, labile iron pools, hemosiderin and ferritin and excretes them in urine [10]. Deferiprone binds excess ferric ions (Fe III) and excretes in urine [11]. Ethylene diamine tetra-acetic acid (EDTA) is used to chelate cadmium, arsenic and mercury [12]. Penicillamine chelates copper, lead and mercury [13] by forming metal complex with divalent cations, which get easily solubilized in water and excreted through urination [14]. Tiron (4,5-Dihydroxy-1,3-benzenedisulphonic acid, disodium salt) is a compound with strong potential to from coordinate complexes with various metal ions. It consists of two hydroxyl groups and two sulfonic acid groups attached in a benzene ring. The attached functional group helps in donating electrons to neutralize free radicals. Tiron alone significantly decreases accumulation of aluminum in brain; however, combination of tiron and glutathione was found better

against aluminum induced toxicity [15]. Individual and combined treatment of tiron with propolis [16] and α-tocopherol, propolis, and piperine [17] were reported to protect liver and kidney from beryllium induced intoxications.

The few studies are available on fabricated nanoparticles of chelating compounds with their biological effects [18]. Tiron, with its immense antioxidant and chelating property due to its structural excellence to donate electron from hydroxyl groups, has never been synthesized as nanoparticles of silver or other metals. Therefore, this investigation aimed fabrication of tiron-loaded silver nanoparticles with physico-chemical and biological characterization for pharmacologically apt properties

2. Materials and methods

2.1 Chemicals: All the chemicals and reagents of analytical grade were used in the study. Silver nitrate, tiron, and aluminum nitrate, were procured from Hi-Media Laboratories, India. Beryllium nitrate was procured from Alpha-Chemika, India.

2.2 Synthesis of tiron-loaded silver nanoparticles: Silver nitrate solution (8 mM) was prepared by dissolving silver nitrate crystals in deionized water and stored in an amber colored bottle. Tiron (4 mM /5 mL) was dissolved in deionized water and maintained *p*H of 10.5 at room temperature; added freshly prepared silver nitrate solution and placed on a magnetic stirrer for 2 hours. Conversion of colorless solution into golden yellow color indicated completion of synthesis of tiron-loaded nanoparticles. Obtained suspension was further centrifuged for 20 min at 10,000 rpm and washed thrice with deionized water to collect nanoparticle pellets, which were dried in an oven at 37° C and kept at 4° C for physico-chemical and biological characterization [19].

2.3 Physico-chemical characterization of tiron-loaded silver nanoparticles

2.3.1 UV-visible spectroscopy

The UV-visible spectroscopy is based on the absorption of ultraviolet or visible light, which excites electrons from lower to higher energy level. The amount of light absorbed at specific wavelength was determined by Beer-Lambert law. During synthesis of tiron-loaded silver nanoparticles, silver ions are reduced from Ag^{+} to Ag^{0}, which was confirmed by scanning the solution of nanoparticles at wavelength 400–500 nm with distilled water as reference. The wavelength range of tiron-loaded silver nanoparticles was determined using a UV-visible spectrophotometer (Systronics, UV-VIS Spectrophotometer Model 117).

2.3.2 Scanning electron microscopy (SEM) with energy dispersive X-ray (EDX)

The SEM works by focusing a beam of high energy electrons onto surface of samples and detecting signals produced by the interaction of beam with the sample, which are used to form high a resolution image showing surface topography and composition. Surface topography of nanoparticles was examined by SEM. The purity of tiron-loaded silver nanoparticles and its aggregation with tiron was inferred from SEM. The SEM (NOVA NANO SEM 450 FEI CO. OF USA (S.E.A.) PTE LTD., SINGAPORE) was

operated with an accelerating voltage of 20.0 kV. The EDX analyzed the surface elemental composition in a sample.

2.3.3 Transmission electron microscopy (TEM)

The principle of TEM is based on transmitting a beam of high energy electrons through a thin layered sample. The transmitted electrons from the sample are used to form a highly magnified image exhibiting internal structure and morphology. Internal morphology of silver nanoparticles was observed under TEM (G2F30 S-Twin at 300kV), which assured the size, morphology, and fabrication of silver nanoparticles.

2.3.4 Particle size analysis (PSA)

Particle size analysis provides average size information of nanoparticles without damaging their property. It relies on the interaction of light energy with particles, or separating particles based on their size and density. The particle size and its distribution were determined using particle size analyzer (METROHM AU B B.V., NETHERLANDS).

2.3.5 Zeta potential

Zeta potential determines the electrical charge on particles surface dispersed in a liquid. It provides potential stability of colloidal system and measures electrostatic repulsion/ attraction between the particles. The zeta potential analysis is used to predict long-term stability of nanoparticles in solution. Zeta potential of tiron-loaded silver nanoparticles was analyzed with the help of zeta potential analyzer, NanoPlus.

2.3.6 Thermogravimetric analysis

Thermogravimetric analysis determined thermal stability and strength of catalysts in nanoparticles by measuring weight/mass change with respect to time and temperature. These mass changes reveal thermal stability, composition and decomposition properties of sample. Differential scanning calorimetry (DSC) measures temperature difference between a sample and a reference material as they are heated or cooled. The instrument used to analyze thermogravimetry of nanoparticles was NETZSCH STA 449F1 STA449F1A-01.

2.3.7 Fourier Transform Infrared Spectroscopy (FTIR)

The FTIR works by passing infrared light through a sample and measuring the absorbed wavelengths. It converts the raw data into a spectrum, providing molecular structure and functional groups in samples. The FTIR spectrum provides absorption peaks in relation to frequencies of vibration within the atoms of nanoparticles. It characterizes nature of material and functional groups present in samples. Functional groups responsible for Ag^{+} reduction, capping/stability of silver nanoparticles were determined with FTIR (SN 340, BRUKER OPTIK GmbH, GERMANY).

2.4 Free radical scavenging activity of tiron-loaded silver nanoparticles

2.4.1 Hydrogen peroxide scavenging activity:

Hydrogen peroxide (H_2O_2) scavenging activity was performed [20] on tiron-loaded silver nanoparticles at concentrations of 2, 4, 6, 8 and 10 µg that was added to 0.1 M phosphate buffer (pH 7.4) and mixed with

43 mM hydrogen peroxide. After 10 min, absorbance of reaction mixture was recorded at λ 230. Ascorbic acid was taken as standard.

$$H_2O_2 \text{ inhibition capacity } (\%) = \frac{A_b - A_a}{A_b} X100$$

Where A_b represents blank and A_a represents absorption of sample

2.4.2 The DPPH free radical scavenging activity:

The 2,2-diphenyl-1-picrylhydrazyl (DPPH) free radical scavenging assay was performed [21]. Samples at different concentrations of 2, 4, 6, 8, 10 and 12 µg of nanoparticle samples of which 100 µl concentration solution sample was added to DPPH solution of 0.3 mM in methanol/ethanol. When sample was added to DPPH solution, the change of color was observed from dark purple to pale yellowish and brownish color, which confirmed that the compound pertains antioxidant property. After 30 min. of incubation in the dark, absorbance of reaction mixture was recorded by spectrophotometer at λ 517 nm. Ascorbic acid was taken as standard.

$$\text{DPPH inhibition capacity } (\%) = \frac{A_b - A_a}{A_b} X\ 100$$

Where A_b represents blank and A_a represents absorption of sample

2.4.3 The ABTS free radical scavenging activity:

The 2,2'-azino-bis-3-ethylbenzothiazoline-6-sulfonic acid (ABTS) assay was performed [22]. The ABTS stock solution was prepared by adding 7 mM ABTS solution with 2.45 mM potassium persulfate solution reacted for 12 hours in the dark at room temperature. The 2 mL of ABTS stock solution was diluted with 50 mL ethanol. Sample at concentrations of 2, 4, 6, 8 and 10 µg was taken. Samples of 300 µl concentration was added to 180µl of ABTS stock solution. When sample was added with ABTS solution, the greenish-blue color of ABTS solution turned colorless in contact with sample molecules, which confirmed antioxidative capacity of the compound. The absorbance was recorded after 5 min. of incubation at λ 734 nm.

$$\text{ABTS inhibition capacity } (\%) = \frac{A_b - A_a}{A_b} X\ 100$$

Where A_b represents blank and A_a represents absorption of sample

2.5 Animal maintenance and lymphocyte culture

Adult female Wistar rats (8–10 weeks old, 150 ± 10 g of body weight) were housed in disinfected polypropylene cages under controlled conditions (14 h light/10 h dark cycle, 25 ± 2°C, 55–70% humidity) with free access to standard pelleted diet (Akhoorath Ventures, Dehradun) and water *ad libitum*. Peripheral blood was taken from rats and lymphocytes were isolated and cultured in RPMI culture media for 24 h.

2.6 *In-vitro* cytoprotective and geno-protective potential of tiron-loaded silver nanoparticles

Cytoprotective potential of was carried with MTT assay and geno-protective potential (DNA damage) with comet assays. Cultured lymphocytes were transferred to 96-well plates and their viability was assessed using the trypan blue exclusion method [23]. The entire well plate was assigned into seven groups. Group 1 served as control that did not receive any treatment, group 2 received co-exposure to combination of Al (1 µg/ml) and Be (6.5 µg/ml), group 3 received tiron-loaded silver nanoparticles 1 µg/ml along with combination of toxicants, group 4 received tiron-loaded silver nanoparticles 2 µg/ml along with combination of toxicants, group 5 received tiron-loaded silver nanoparticles 3 µg/ml along with combination of toxicants, group 6 received tiron-loaded silver nanoparticles 4 µg/ml along with combination of toxicants, group 7 received tiron-loaded silver nanoparticles 5µg/ml along with combination of both toxicants and incubated at 37° C for 24 h [24].

The MTT assay

After 24 h of incubation, cells were treated with 5 mg/ml solution of diphenyltetrazolium bromide (MTT) for 4 h. Afterward, 100 µl of dimethyl sulfoxide (DMSO) was added to dissolve violet crystals [25]. The absorbance was determined by a microplate reader at λ 532 nm, and cell viability was determined with following formula, where C represents the absorbance of the control group and T is the absorbance of the treated group.

Cell viability (%) = (C − T)/C × 100

Comet assay

The comet assay was performed on lymphocytes in seven groups as mentioned in MTT assay [26]. The cell suspension was combined with an equal amount of 1% low-melting-point agarose and layered onto clean glass slides that had been pre-coated with 1% normal-melting-point agarose. Following electrophoresis, the slides were stained with ethidium bromide solution (1.5 mg/ml), and comet images were captured in bitmap format with fluorescence microscope (Leica DM-2500. Different parameters, including comet length, height, area, head diameter, % DNA in head, tail length, tail area, % DNA in tail, tail moment, and olive tail moment were analyzed. The mean values were calculated using TriTek comet analysis software.

2.7 Statistical analysis

The data were expressed as mean ± standard error (SE). Statistical significance was analyzed with one-way ANOVA with a significance level at $p \leq 0.05$ followed by Tukey's HSD post hoc test at $p \leq 0.05$ to compare differences between multiple groups.

3. Results

3.1 Characterization of tiron-loaded silver nanoparticles

3.1.1 Synthesis of tiron-loaded silver nanoparticles

At the end point of synthesis, change in color from colorless to golden yellow confirmed the synthesis of tiron-loaded silver nanoparticles. Tiron molecules donate electrons to silver ions (Ag^{+}) in the solution to reduce them into Ag^{0} that leads to nucleation and growth into nanoparticles (Fig. 1a, b).

3.1.2 UV-visible spectroscopy

UV- visible spectroscopy confirmed the formation of tiron-loaded silver nanoparticles showing absorbance peak at 430–440 nm. The peak refers to a specific optical property of synthesized tiron-loaded silver nanoparticles as a stabilizing or reducing agent and its presence can greatly influence the size, shape and optical properties of silver nanoparticles (Fig. 1d)

3.1.3 Scanning electron microscope (SEM) with energy dispersive X-ray

In SEM, it was remarkably observed that the nanoparticles were primarily spherical and more or less elongated in shape. Field emission SEM images of tiron-loaded silver nanoparticles at 4μm scale with HV 10.00 kV and working distance of 6.3 mm at 20000X magnification showing spherical shape nanoparticles (Fig. 2a). The EDX analysis of tiron-loaded silver nanoparticles with dominated silver element (red dot) over the samples (Fig. 2b). Figure 2c demonstrates the EDX analysis of tiron-loaded silver nanoparticles with sharp peak at 2.60 keV energy level.

3.1.4 Transmission electron microscope (TEM)

The TEM provided complete information of size, distribution and morphological background of nanoparticles. Figure 3a showed selected area electron diffraction (SAED) pattern. The concentric rings with dots indicating crystalline nature of nanoparticles add plane. In this pattern, the nanoparticles exhibited polycrystalline nature and face centered cubic structure. The average size of silver nanoparticles in terms of area is 21.94093 nm. Figure 3b illustrated spherical shaped silver nanoparticles with size area ranging from 5–50 nm. Figure 3c & d exhibited high resolution polycrystalline lattice fringes at 10 nm scale with visible lattice planes. Polycrystalline denotes that the materials of nanoparticles are composed of multiple small crystalline grains. The lattice fringes exhibit

regular and periodic patterns of contrast, which result from diffraction of electrons passing through the crystalline lattice of the nanoparticle material.

3.1.5 Particle size analysis

The average size diameter in length of nanoparticles synthesized from tiron was 14.9, 109.4, 1305.5, and 12143.7 nm implies broad range of particle sizes. Different particle size shows nucleation and growth of nanoparticles. Particle size 14.9 nm could be the newly formed nuclei while 109.4, 1305.5, and 12143.7 nm could represent subsequent growth stages and aggregation within the nanoparticles. Figure 4a showed size dispersion of tiron-loaded silver nanoparticles with intensity. The nanosize diameter indicated that tiron has strong capacity to reduce silver during nanoparticle synthesis.

3.1.6 Zeta potential

The zeta potential of synthesized tiron-loaded silver nanoparticles was determined in water as diluent. The zeta potential was found to be -98.17mV. High negative charge confirmed the higher electrostatic repulsion within the particles preventing them aggregation and showed higher stability of nanoparticle formulation and extremely stable colloidal dispersion. The high negative zeta potential revealed that the surface of silver nanoparticles was strongly negatively charged as shown in Fig. 4b.

3.1.7 Thermogravimetric analysis

Thermogravimetric analysis/ differential scanning colorimetry (TG/ DSC) of tiron-loaded silver nanoparticles are shown within temperature range from 20° C to 560° C as displayed in Fig. 5. Initial weight loss obtained at 100° C was 21.98% due to evaporation of water adsorbed by the silver nanoparticles. Second weight loss obtained at 180° C was 5.4% and ended weight loss was marked at 540° C, which showed that tiron compound present in nanoparticles get decomposed successfully. The total weight loss was around 27.38%. The results of DSC curve illustrated sharp exothermic peak at 142.7° C along with appearance of endothermic peak at 162° C. The exothermic peak indicated flow of less heat towards the sample while endothermic peak showed flow of more heat towards the sample. Exothermic peak at 142.7° C represented crystallization of silver nanoparticles and could be transitioning from amorphous particles to more ordered crystalline structured particles.

3.1.8 The FTIR analysis

Presence of different functional groups in a compound determines the chemical reactions, reduction, capping/ stability of the compound. The FTIR spectrum of tiron-loaded silver nanoparticles was taken recorded. Various band range was found between 500 and 4000 absorption spectra as shown in Fig. 6. Absorption spectra of 3776.68 cm^{-1} showed the presence of hydroxyl group (-OH) stretching vibration with broad peak bound to tiron-loaded silver nanoparticles. Band at 3687.08, 3655.36 and 3627.75 cm^{-1} assigned to (-OH) stretching alcohol group with medium sharp peak and 1589.21 cm^{-1} revealed cyclic alkene (C = C) stretching with medium peak.

3.2 Free radical scavenging activity of tiron-loaded silver nanoparticles

3.2.1 Hydrogen peroxide scavenging activity

Tiron-loaded silver nanoparticles showed concentration dependent H_2O_2 free radical scavenging activity at different concentrations of 2, 4, 6, 8, and 10 µg. Increasing order of concentration of nanoparticles exhibited increasing order of H_2O_2 free radical scavenging activity (Fig. 7a). The IC_{50} value of tiron-loaded silver nanoparticles was recorded as 6.183 µg.

3.2.2 The DPPH free radical scavenging activity

Tiron-loaded silver nanoparticles showed concentration dependent DPPH free radical scavenging activity at different concentrations of 2, 4, 6, 8, 10 and 12 µg. The increasing order of concentration of tiron-loaded silver nanoparticles showed high DPPH free radical scavenging activity, which assured its antioxidative property at increasing concentrations (Fig. 7b). The IC_{50} value of tiron-loaded silver nanoparticles against DPPH free radical assay was noted as 4.317 µg.

3.2.3 The ABTS free radical scavenging activity

Tiron-loaded silver nanoparticles also exhibited concentration dependent ABTS free radical scavenging activity at 2, 4, 6, 8, and 10 µg concentrations. The increasing order of concentration of tiron-loaded silver nanoparticles showed increasing order of ABTS free radical scavenging activity, which assured its increasing antioxidative potential at increasing concentrations (Fig. 7c). The IC_{50} value of tiron-loaded silver nanoparticles against DPPH free radical assay was noted as 1.021µg.

3.3 Cell viability assay

In vitro cell viability study was performed with MTT assay. After 4 h of incubation period, significant difference was noted among control, toxicants and different treatment groups. Control group showed regular cytotoxicity, whereas combination of aluminum and beryllium significantly increased cytotoxicity of lymphocytes. The tiron-loaded silver nanoparticles at different concentrations 1,2,3,4 and 5 µg/ml with co-exposure to Al and Be significantly decreased cytotoxicity, thus increased viability of lymphocytes (Fig. 8a)

3.4 Geno-protective potential of tiron-loaded silver nanoparticles

To determine geno-protective potential of tiron-loaded silver nanoparticles, comet assay was performed. The comet assay signified that combined exposure to Al and Be significantly increased genotoxicity as indicated by increase in tail length as compared to control group. Tiron-loaded silver nanoparticles at concentrations of 1, 2, 3, 4 and 5 µg/ml along with combined exposure to Al and Be offered protection to

DNA as indicated by decrease in tail length (Fig. 8b). Different parameters of comet assays, including comet length, comet height, comet area, head diameter, % DNA in head, tail length, tail area, % DNA in tail, tail movement, and olive moment have been given in Table 1. Figure 9 and Table 1 jointly represented that tiron-loaded silver nanoparticles have excellent potential to protect DNA from damage; thus, reduced genotoxicity.

Table 1
Geno-protective potential of TAgNPs using comet assay

Parameter	Control	Al + Be	TAgNPs 1mg	TAgNPs 2mg	TAgNPs 3mg	TAgNPs 4mg	TAgNPs 5mg	ANOVA (F-value)
Comet length	136 ± 7.51	677 ± 37.4^{a}	297 ± 16.4^{ab}	250 ± 13.8^{ab}	221 ± 12.2^{abc}	185 ± 10.2^{bc}	168 ± 9.28^{bcd}	127$^{@}$
Comet height	103 ± 5.69	605 ± 33.4^{a}	309 ± 17.0^{ab}	260 ± 14.3^{ab}	249 ± 13.7^{ab}	198 ± 10.9^{abc}	180 ± 9.95^{abcd}	106$^{@}$
Comet area	47 ± 2.59	484 ± 26.7^{a}	311 ± 17.1^{ab}	252 ± 13.9^{abcd}	71 ± 3.92^{bcd}	58 ± 3.20^{bcd}	71 ± 3.92^{bcd}	191$^{@}$
Head diameter	51 ± 2.81	96 ± 5.30^{a}	166 ± 9.17^{ab}	176 ± 9.72^{ab}	59 ± 3.26^{bcd}	93 ± 5.14^{acde}	103 ± 5.69^{acde}	68.9$^{@}$
% DNA in head	100 ± 5.52	20.3 ± 1.12^{a}	91.5 ± 5.05^{b}	92.3 ± 5.10^{b}	93.1 ± 5.14^{b}	93.4 ± 5.16^{b}	99.1 ± 5.48^{b}	40.6$^{@}$
Tail length	02 ± 0.11	818 ± 45.2^{a}	19 ± 1.05^{b}	15 ± 0.82^{b}	10 ± 0.55^{b}	05 ± 0.27^{b}	03 ± 0.16^{b}	384$^{@}$
Tail area	02 ± 0.11	51 ± 2.81^{a}	13 ± 0.71^{ab}	11 ± 0.60^{ab}	07 ± 0.38^{abc}	02 ± 0.11^{bcde}	01 ± 0.05^{bcde}	290$^{@}$
% DNA in tail	11.9 ± 0.66	97.4 ± 5.38^{a}	11 ± 0.60^{b}	10 ± 0.55^{b}	0.01 ± 0.00^{bcd}	9.62 ± 0.53^{be}	4.44 ± 0.24^{b}	321$^{@}$
Tail movement	0	939 ± 51.9^{a}	5 ± 0.27^{b}	6 ± 0.33^{b}	3 ± 0.16^{b}	2 ± 0.11^{b}	2 ± 0.11^{b}	390$^{@}$
Olive movement	0	109 ± 6.02^{a}	4 ± 0.22^{b}	7 ± 0.38^{b}	5 ± 0.27^{b}	4 ± 0.22^{b}	1 ± 0.05^{b}	366$^{@}$

Data are presented at mean ± SE, *control vs Al + Be at P ≤ 0.05, TAgNPs + (Al + Be) for tukey's HSD post hoc test at P ≤ 0.05; Significant at 5% level for ANOVA. Abbreviation: Al + Be (aluminium + beryllium) at 1 µg + 6.5 µg, TAgNPs = Tiron loaded silver nanoparticles at 1–5 mg; ^{a}Control vs Al + Be, TAgNPs 1–5 mg/kg, ^{b}Al+Be vs TAgNPs 1–5 mg/kg, ^{c}TAgNPs 1 mg/kg vs TAgNPs 2–5 mg/kg, ^{d}TAgNPs 2 mg/kg vs TAgNPs 3–5 mg/kg, ^{e}TAgNPs 3 mg/kg vs TAgNPs 4–5 mg/kg, ^{f}TAgNPs 4 mg/kg vs TAgNPs 5 mg/kg

4. Discussion

Tiron (4,5-dihydroxy-1,3-benzenedisulfonic acid disodium salt) has been reported as an excellent chelator and therapeutic agent against aluminum [15, 27] and beryllium [16, 17, 28] induced toxic manifestations. Silver nanoparticles of various compounds exhibit antimicrobial, bactericidal, anticancer, and wound-healing properties [29]. Synthesis of tiron-loaded silver nanoparticles may offer an innovative approach against combined exposure to Al and Be induced toxic manifestations in liver and kidney. Tiron, acted as reducing and capping agent during synthesis of silver nanoparticle, contributing antioxidant properties to the nanoparticles by chelating metals and scavenging reactive oxygen species (ROS). Tiron stabilizes nanoparticles and prevents aggregation and form smaller uniform particles. Presence of hydroxyl group, stretched alcohol group and cyclic alkenes primarily contribute to reduction of Ag^{+} ion forming tiron-loaded silver nanoparticles. Chelating and antioxidant properties of tiron protect liver [28], kidney [28] and brain [15] from metal toxicity. In view of this, the present work aimed to synthesize and characterize tiron-loaded silver nanoparticles and evaluate their *in vitro* antioxidant and protective activity against toxicity induced by combined exposure to Al and Be.

The change in color of tiron-loaded AgNPs was relevant to the change in color noticed in econazole nitrate synthesized silver nanoparticles [30]. This change was attributed to the surface plasmon resonance of silver nanoparticles, and the color intensity corresponds to the number of electrons released during the reduction of Ag^{+} to Ag^{0} [31, 32].

Tiron loaded silver nanoparticles revealed surface plasmon resonance shifting, which confirmed interaction of tiron on the surface of silver nanoparticle. The observed peak at wavelength 430–440 nm was a characteristic feature of silver nanoparticles as reported in previous findings [33]. Spherical shape of silver nanoparticles indicated uniform nucleation and growth, which exhibited homogenous size distribution [34]. Spherical shape offers enhanced cellular uptake of silver nanoparticles, may improve circulation and biodistribution with more predictable and controlled drug release [35]. Its interaction with tiron could enhance pharmacological performance. The EDX analysis confirmed the presence of silver metal ions, which dominated surface of the samples that indicated the capping of silver nanoparticles with tiron. The EDX spectrum indicated prominent signal for silver metals. This analysis was relevant to earlier work [36]. In the present study, tiron-loaded silver nanoparticles showed promising potential in drug delivery and size uniformity as analyzed and confirmed by TEM. The average size area of silver nanoparticles often shows increased surface area with effective biological interactions. The spherical shape ensures uniform distribution and good biocompatibility. The average size of tiron-loaded silver nanoparticles in terms of area was found 21.94093 nm while spherical shaped with size area was in a range from 5–50 nm. Presence of lattice fringes showed polycrystalline nature, which provides stability, reactivity and electron sharing ability. Polycrystalline structure of tiron-loaded silver nanoparticles was due to rapid nucleation, growth and stabilization of growing nanoparticles. Tiron inhibited aggregation and growth rate by acting as a capping agent resulting in polycrystallinity, which enhanced surface activity and reactivity of silver nanoparticles leading their potential use in pharmacology [37, 38]. Particle size analysis of tiron-loaded silver nanoparticles manifested broad size distribution 109.4, 1305.5, and

12143.7 nm can occur due to agglomeration over specific area or variations in parameters such as pH, temperature and reaction time [39, 40, 41]. This reflected the hydrodynamic diameter of capping agent and solvation layer around the particles which makes them suitable for drug delivery.

Zeta potential of nanoparticles provides an important information about their surface charge and stability in suspension and electrostatic repulsion or attraction among the nanoparticles. In this investigation, zeta potential was observed – 98.17mV, which indicated high stability with high repulsion between the nanoparticles. Tiron having two hydroxyl and sulfonate groups, strongly ionize in solvent media, resulting in negatively charged surface showing colloidal stability due to impact arrangement of tiron molecules or strong chelation. This could be due to the highly negative charged stabilizers or functional groups adsorbed on the surface of nanoparticles [42, 43].

The TGA helps in monitoring of sample in terms of weight loss with respect to temperature. In tiron-loaded silver nanoparticles, initial weight loss indicated adsorbed water and loosely bound surface molecules (volatile molecules). Secondary weight loss reflected partial decomposition of weakly organic molecules and final decomposition results in complete degradation of tiron at 540℃ [44, 45]. The sharp exothermic peak of DSC curve revealed oxidative decomposition while endothermic peak at 162 ℃ signified thermal disruptions among the molecules. This study confirmed that tiron-loaded silver nanoparticles revealed complete decomposition and crystallization of the nanoparticles. This thermostability supports its suitability for pharmaceutical application.

Tiron-loaded silver nanoparticles showed specified functional groups, including hydroxyl groups and cyclic alkene [46, 47, 48]. This suggested multiple functional groups participated in reducing, capping and stabilization of tiron-loaded silver nanoparticles and also raised solubility, antioxidant activity and bio-interaction of nanoparticles and enhanced its applications for pharmaceutical uses [49]. Tiron showed its significant applications in both pharmacy and pharmaceutical industries due to their specific complex formation with toxic metals [15] inhibiting ROS generation and minimizing oxidative stress and cellular injury [50]. This features primarily showed its antioxidant and metal chelating property [51]. The H_2O_2, DPPH and ABTS induced free radical scavenging activity of tiron-loaded silver nanoparticles corroborated its potential as an excellent antioxidant for medicinal uses.

The *in vitro* safety profile assessment provided an alternative method of animal testing for evaluating toxicological and/ or therapeutic effects of chemical entities. Combined exposure to Al and Be to lymphocytes has been implicated in producing damage to mitochondria and its dysfunction [52, 53]. Combination of Al and Be disrupted cellular redox system by prompting oxidative stress, mitochondrial dysfunctions and alteration in DNA entity. It is further associated with the initiation of lipid peroxidation process and cytoplasmic enzymes leakage like lactate dehydrogenase and transaminases showing disturbance in membrane integrity [54]. The hydroxyl and sulfonate groups in tiron play crucial role in metal binding. Tiron-loaded silver nanoparticles exhibited remarkable antioxidant probably through its metal-chelating behavior. Cellular macromolecules such as lipids, proteins and DNA were negatively affected when exposed to Al and Be [55]. Tiron-loaded silver nanoparticles possess unique

physicochemical characteristics that could help in preventing oxidative stress and DNA damage caused by free radicals and contribute to the stabilization of both cell membranes and DNA itself.

5. Conclusion

This study concluded that tiron-loaded silver nanoparticles may offer excellent therapeutic potential at relatively lower doses in comparison to previously used doses of tiron alone. Tiron-loaded silver nanoparticles have pharmacologically apt physico-chemical and biological properties; thus, may offer as a promising agent for medicinal use against combination of Al and Be induced toxic manifestations in terms of oxidative stress associated disorders.

Declarations

The study was approved by institutional animal ethics committee (CPCSEA/994/GO/Re/S/06).

Conflict of interest:

The authors declare no competing interests.

Funding:

Partial financial support from Guru Ghasidas University by providing non-NET fellowship to PD, PB, AM and AAS and for procuring selected chemicals.

Author Contribution

PD, PB AM and AAS collectively done bench work of the experiment, PD prepared draft of the manuscript, SKN and MB conceptualized and prepared experimental design, arranged essential facilities, materials and supervision to complete the experimentation.

Data Availability

No datasets were generated or analyzed during the current study.

References

1. Durgam, L. K., & Oroszi, T. L. (2025). Revolutionizing healthcare: the transformative potential of nanotechnology in medicine. *Frontiers in Drug Delivery*, *5*, 1556426. https://doi.org/10.3389/fddev.2025.1556426

2. Ritu Verma, K. K., Das, A., & Chandra, P. (2023). Phytochemical-based synthesis of silver nanoparticle: mechanism and potential applications. *BioNanoScience*, *13*(3), 1359–1380. https://doi.org/10.1007/s12668-023-01125-x
3. Elabed, S., Sheirf, A., & Ali, M. (2025). Nanostructures for cancer therapeutics and diagnostics: Recent advances and future outlook. *Radiation Physics and Chemistry*, *226*, 112295. https://doi.org/10.1016/j.radphyschem.2024.112295
4. Bukke, S. P. N., Venkatesh, C., Bandenahalli Rajanna, S., Saraswathi, T. S., Kusuma, P. K., Goruntla, N., & Munishamireddy, S. (2024). Solid lipid nanocarriers for drug delivery: design innovations and characterization strategies—a comprehensive review. *Discover applied sciences*, *6*(6), 279. https://doi.org/10.1007/s42452-024-05897z
5. Sayed, A., Hiekal, A. S., Moussa, S. I., Aydia, M. I., El-Sabagh, H. A., Mahmoud, G. A., & El-Azony, K. M. (2025). Preparation and Characterization of Silver Ferrite Nanoparticles (AgFeO2) and Investigation of Their Cytotoxicity Properties. *BioNanoScience*, *15*(3), 353. https://doi.org/10.1007/s12668-025-01974-8
6. Ni, F., Lv, H., Lin, L., Zhang, Y., Qiao, Y., Zhang, X., & Dong, J. (2025). Antitumor/anti-inflammatory effects/tissue healing as an all-in-one therapeutic strategy for nasopharyngeal carcinoma. *Journal of Nanobiotechnology*, *23*(1), 431. https://doi.org/10.1186/s12951-025-03520-w
7. Oselusi, S. O., Sibuyi, N. R., Meyer, M., & Madiehe, A. M. (2024). Phytonanotherapeutic applications of plant extract-synthesized silver nanoparticles in wound healing—A prospective overview. *BioNanoScience*, *14*(3), 3455–3475. https://doi.org/10.1007/s12668-024-01535-5
8. Ramos-Hernandez, R., Gonzalez-Diaz, F., Salas-Tellez, E., Sordo, M., Salazar, A. M., Ostrosky-Wegman, P., & Vazquez-Duran, A. (2025). Within and Beyond the MIC: Unveiling the Antifungal Potency of Green-Synthesized Silver Nanoparticles Against Clinical Isolates of Candida albicans. *BioNanoScience*, *15*(3), 407. https://doi.org/10.1007/s12668-025-02030-1
9. Chaudhary, M., & Singh, A. (2024). Synthesis of Nanoparticles Using Fruit Waste and Its Pharmacological & Catalytic Applications: A Review. *BioNanoScience*, *14*(4), 3830–3845. https://doi.org/10.1007/s12668-024-01550-6
10. Zhu, D., Liang, R., Liu, Y., Li, Z., Cheng, L., Ren, J., & Qin, X. (2022). Deferoxamine ameliorated Al (mal) 3-induced neuronal ferroptosis in adult rats by chelating brain iron to attenuate oxidative damage. *Toxicology mechanisms and methods*, *32*(7), 530–541. https://doi.org/10.1080/15376516.2022.2053254
11. Rashed, R. R., Deghiedy, N. M., El-Hazek, R. M., El-Sabbagh, W. A., Rashed, E. R., & El-Ghazaly, M. A. (2020). Effectiveness of deferiprone-loaded nanocarrier in experimentally induced rhabdomyolysis: A dose-comparison study. *Bioorganic Chemistry*, *100*, 103913. https://doi.org/10.1016/j.bioorg.2020.103913
12. Flora, S. J. S., Mittal, M., & Mehta, A. (2008). Heavy metal induced oxidative stress & its possible reversal by chelation therapy. *Indian Journal of Medical Research*, *128*(4), 501–523. 128(4):p 501–523, October 2008.

13. Cao, Y., Skaug, M. A., Andersen, O., & Aaseth, J. (2015). Chelation therapy in intoxications with mercury, lead and copper. *Journal of Trace Elements in Medicine and Biology*, *31*, 188–192. https://doi.org/10.1016/j.jtemb.2014.04.010
14. Kuchinskas, E. J., & Rosen, Y. (1962). Metal chelates of DL-penicillamine. *Archives of Biochemistry and Biophysics*, *97*(2), 370–372. https://doi.org/10.1016/0003-9861(62)90090-5
15. Sharma, P., Shah, Z. A., Kumar, A., Islam, F., & Mishra, K. P. (2007). Role of combined administration of Tiron and glutathione against aluminum-induced oxidative stress in rat brain. *Journal of Trace Elements in Medicine and Biology*, *21*(1), 63–70. https://doi.org/10.1016/j.jtemb.2006.12.001
16. Nirala, S. K., Bhadauria, M., Shukla, S., Agrawal, O. P., Mathur, A., Li, P. Q., & Mathur, R. (2008). Pharmacological intervention of tiferron and propolis to alleviate beryllium induced hepatorenal toxicity. *Fundamental & clinical pharmacology*, *22*(4), 403–415. https://doi.org/10.1111/j.1472-8206.2008.00603.x
17. Nirala, S. K., Bhadauria, M., Mathur, R., & Mathur, A. (2008). Influence of α-tocopherol, propolis and piperine on therapeutic potential of tiferron against beryllium induced toxic manifestations. *Journal of Applied Toxicology: An International Journal*, *28*(1), 44–54. https://doi.org/10.1002/jat.1250
18. Jung, W., Lee, D. Y., Moon, E., & Jon, S. (2022). Nanoparticles derived from naturally occurring metal chelators for theranostic applications. *Advanced Drug Delivery Reviews*, *191*, 114620. https://doi.org/10.1016/j.addr.2022.114620
19. Singh, S., Nirala, S. K., Kumar, D., Shukla, S., Shrivastava, S., & Bhadauria, M. (2024). Physicochemical characterization and *In vitro* biological activity of silver nanoparticles of Propolis extract. *BioNanoScience*, *14*(3), 2181–2196. https://doi.org/10.1007/s12668-024-01469-y
20. Ruch, R. J., Cheng, S. J., & Klaunig, J. E. (1989). Prevention of cytotoxicity and inhibition of intercellular communication by antioxidant catechins isolated from Chinese green tea. *Carcinogenesis*, *10*(6), 1003–1008. https://doi.org/10.1093/carcin/10.6.1003
21. Gulcin, İ., & Alwasel, S. H. (2023). DPPH radical scavenging assay. *Processes*, *11*(8), 2248. https://doi.org/10.3390/pr11082248
22. Rumpf, J., Burger, R., & Schulze, M. (2023). Statistical evaluation of DPPH, ABTS, FRAP, and Folin-Ciocalteu assays to assess the antioxidant capacity of lignins. *International Journal of Biological Macromolecules*, *233*, 123470. https://doi.org/10.1016/j.ijbiomac.2023.123470
23. Ghosh, M., Bandyopadhyay, M., & Mukherjee, A. (2010). Genotoxicity of titanium dioxide (TiO2) nanoparticles at two trophic levels: plant and human lymphocytes. *Chemosphere*, *81*(10), 1253–1262. 10.1016/j.chemosphere.2010.09.022
24. Kumar, V., Sharma, N., & Maitra, S. S. (2017). In vitro and in vivo toxicity assessment of nanoparticles. *International Nano Letters*, *7*(4), 243–256. https://doi.org/10.1007/s40089-017-0221-3
25. Ghosh, M., Chakraborty, A., & Mukherjee, A. (2013). Cytotoxic, genotoxic and the hemolytic effect of titanium dioxide (TiO2) nanoparticles on human erythrocyte and lymphocyte cells in vitro. *Journal of applied toxicology*, *33*(10), 1097–1110. https://doi.org/10.1002/jat.2863

26. Ojemaye, M. O., Okoh, S. O., & Okoh, A. I. (2021). Silver nanoparticles (AgNPs) facilitated by plant parts of Crataegus ambigua Becker AK extracts and their antibacterial, antioxidant and antimalarial activities. *Green Chemistry Letters and Reviews*, *14*(1), 51–61. https://doi.org/10.1080/17518253.2020.1861344
27. Sharma, P., & Mishra, K. P. (2006). Aluminum-induced maternal and developmental toxicity and oxidative stress in rat brain: response to combined administration of Tiron and glutathione. *Reproductive Toxicology*, *21*(3), 313–321. https://doi.org/10.1016/j.reprotox.2005.06.004
28. Nirala, S. K., Bhadauria, M., Upadhyay, A. K., Mathur, R., & Mathur, A. (2009). Reversal of effects of intra peritoneally administered beryllium nitrate by tiron and $CaNa_3$DTPA alone or in combination with-tocopherol. 10.56042/ijeb
29. Jangid, H., Singh, S., Kashyap, P., Singh, A., & Kumar, G. (2024). Advancing biomedical applications: an in-depth analysis of silver nanoparticles in antimicrobial, anticancer, and wound healing roles. *Frontiers in pharmacology*, *15*, 1438227. https://doi.org/10.3389/fphar.2024.1438227
30. Abdel-Magied, N., Abdel-Aziz, N., Shedid, S. M., & Ahmed, A. G. (2019). Modulating effect of tiron on the capability of mitochondrial oxidative phosphorylation in the brain of rats exposed to radiation or manganese toxicity. *Environmental Science and Pollution Research*, *26*, 12550–12562. https://doi.org/10.1007/s11356-019-04594-4
31. Sawant, P., Chopade, S., Shrotriya, S., Patil, M., & Mulgund, S. (2025). Controlled Size Silver Nanoparticles Stabilised with Trisodium Citrate as Carriers for Econazole Nitrate: Synthesis, Characterization and Antifungal Activity. *BioNanoScience*, *15*(2), 265. https://doi.org/10.1007/s12668-025-01874-x
32. Tesfaye, M., Gonfa, Y., Tadesse, G., Temesgen, T., & Periyasamy, S. (2023). Green synthesis of silver nanoparticles using Vernonia amygdalina plant extract and its antimicrobial activities. *Heliyon*, *9*(6). https://doi.org/10.1016/j.heliyon.2023.e17356
33. Fakharzadeh, M., & Fazljoo, S. E. (2024). Biosynthesis of Silver Nanoparticles using Barley straw and Fumaria parviflora extract: Optimization of synthesis, Evaluating of Nanoparticles stability, Antibacterial activities. *Bionanoscience*, *14*(1), 318–336. https://doi.org/10.1007/s12668-023-01242-7
34. Atanda, S. A., Shaibu, R. O., & Agunbiade, F. O. (2024). Eco-friendly synthesis and antibacterial potential of chitosan crosslinked-EDTA silver nanocomposite (CCESN). *Journal of Materials Science: Materials in Engineering*, *19*(1), 22. https://doi.org/10.1186/s40712-024-00164-w
35. Ogungbesan, S. O., Buxaderas, E., Adedokun, R. A., Moglie, Y., Grijalvo, S., Garcia, M. T., & Fu, G. (2024). Synthesis and Characterization of Chitosan–Silver Nanocomposite Film: Antibacterial and Cytotoxicity Study. *Chemistry Select*, *9*(42), e202404909. https://doi.org/10.1002/slct.202404909
36. Gul, A., Baig, M. N., Ahmed, D., Najam, Z., Aslam, T., & Ali, S. (2024). Green synthesis of silver nanoparticles from Spirulina platensis extract: Antibacterial and antioxidant potential. *BioNanoScience*, *14*(3), 2327–2336. https://doi.org/10.1007/s12668-024-01473-2

37. Deviprasad, M. J., Hemanth, B. S., Shivaswamy, M. B., Nagendra Prasad, H. S., Sumathi, S., Aswathy, R., & Lohith, T. N. (2024). Multifunctional Citral–Tryptamine Conjugated Silver Nanoparticles (CT@ AgNPs): Antibacterial, Cytotoxicity, and Sensor Application. *BioNanoScience*, *14*(5), 5106–5121. https://doi.org/10.1007/s12668-024-01583x
38. Thiruvengadam, V., & Bansod, A. V. (2020). Characterization of silver nanoparticles synthesized using chemical method and its antibacterial property. *Biointerface Res Appl Chem*, *10*, 7257–7264. https://doi.org/10.33263/BRIAC106.72577264
39. Balamurugan, M., Prabhuram, S. R. R., Kumar, G. V., Chamseddine, A., Velusamy, P., Bajaber, M. A., & Gopinath, S. C. (2025). Pseudomonas fluorescens–Based Biogenic Silver Nanoparticles: a Green Solution for Brown Leaf Spot Disease in Rice. *BioNanoScience*, *15*(2), 1–11. https://doi.org/10.1007/s12668-025-01911-9
40. Wahab, A. W., Karim, A., La Nafie, N., & Sutapa, I. W. (2018). Synthesis of Silver Nanoparticles using Muntingia calabura L. Extract as Bioreductor and Applied as Glucose Nanosensor. *Oriental Journal of Chemistry*, *34*(6). http://dx.doi.org/10.13005/ojc/340652
41. Shah, A., Ashames, A. A., Buabeid, M. A., & Murtaza, G. (2020). Synthesis, in vitro characterization and antibacterial efficacy of moxifloxacin-loaded chitosan-pullulan-silver-nanocomposite films. *Journal of Drug Delivery Science and Technology*, *55*, 101366. https://doi.org/10.1016/j.jddst.2019.101366
42. Ali, I. A. M., Ahmed, A. B., & Al-Ahmed, H. I. (2023). Green synthesis and characterization of silver nanoparticles for reducing the damage to sperm parameters in diabetic compared to metformin. *Scientific Reports*, *13*(1), 2256. https://doi.org/10.1038/s41598-023-29412-3
43. Thapa, P., Bachhar, N., & Sarma, S. (2025). Substrate-dependent thermal sensing using silver nanoparticles synthesized via laser ablation in solution. *Scientific Reports*, *15*(1), 23614. https://doi.org/10.1038/s41598-025-02431-y
44. Adebayo-Tayo, B., Salaam, A., & Ajibade, A. (2019). Green synthesis of silver nanoparticle using Oscillatoria sp. extract, its antibacterial, antibiofilm potential and cytotoxicity activity. *Heliyon*, *5*(10). 10.1016/j.heliyon.2019.e02502
45. Nunes, A. M. A., de Oliveira Alves Junior, J., Sato, M. R., Nunes, B. R. P., Macedo, R. O., & Junior, J. A. O. (2025). Synthesis, Physicochemical Characterization, and Antimicrobial Evaluation of Ureasil-Polyether Coatings with Silver Nanoparticles for Hospital Devices. *BioNanoScience*, *15*(2), 305. https://doi.org/10.1007/s12668-025-01920-8
46. FTIR Functional Group Database Table with Search InstaNANO https://instanano.com/all/characterization/ftir/ftir-functional-group-search
47. Lingegowda, D. C., Kumar, J. K., Prasad, A. D., Zarei, M., & Gopal, S. (2012). FTIR spectroscopic studies on cleome gynandra-Comparative analysis of functional group before and after extraction. *Rom J Biophys*, *22*(3–4), 137–143.
48. Ustynyuk, L. Y., Medvedeva, V. A., Liubimovskii, S. O., Ruuge, E. K., & Tikhonov, A. N. (2023). Interaction of Magnesium Ions with Semiquinone Radicals of Tiron, an Indicator of Reactive Oxygen

Species. *Biophysics*, *68*(6), 915–923. https://doi.org/10.1134/S0006350923060192

49. Lakkim, V., Reddy, M. C., Lekkala, V. V., Lebaka, V. R., Korivi, M., & Lomada, D. (2023). Antioxidant efficacy of green-synthesized silver nanoparticles promotes wound healing in mice. *Pharmaceutics*, *15*(5), 1517. https://doi.org/10.3390/pharmaceutics15051517
50. Balali-Mood, M., Eizadi-Mood, N., Hassanian-Moghaddam, H., Etemad, L., Moshiri, M., Vahabzadeh, M., & Sadeghi, M. (2025). Recent advances in the clinical management of intoxication by five heavy metals: Mercury, lead, chromium, cadmium and arsenic. *Heliyon*, *11*(4).10.1016/j.heliyon.2025.e42696.
51. Tonholo, D. R., Maltarollo, V. G., Kronenberger, T., Silva, I. R., Azevedo, P. O., Oliveira, R. B., & Tagliati, C. A. (2020). Preclinical toxicity of innovative molecules: In vitro, in vivo and metabolism prediction. *Chemico-Biological Interactions*, *315*, 108896. https://doi.org/10.1016/j.cbi.2019.108896
52. Skarabahatava, A. S., Lukyanenko, L. M., Slobozhanina, E. I., Falcioni, M. L., Orlando, P., Silvestri, S., & Falcioni, G. (2015). Plasma and mitochondrial membrane perturbation induced by aluminum in human peripheral blood lymphocytes. *Journal of Trace Elements in Medicine and Biology*, *31*, 37–44. https://doi.org/10.1016/j.jtemb.2015.02.002
53. Liu, Z., Wang, K., Yan, Q., Wang, H., Zhang, N., Gong, A., & Guo, X. (2019). Beryllium inhibits apoptosis via mitochondria in beryllium-induced lung disease in the rat. *Experimental Lung Research*, *45*(3–4), 92–100. https://doi.org/10.1080/01902148.2019.1621409
54. Attia, S. M., Harisa, G. I., Hassan, M. H., & Bakheet, S. A. (2013). Beryllium chloride-induced oxidative DNA damage and alteration in the expression patterns of DNA repair-related genes. *Mutagenesis*, *28*(5), 555–559. https://doi.org/10.1093/mutage/get032
55. Czarny, P., Wigner, P., Galecki, P., & Sliwinski, T. (2018). The interplay between inflammation, oxidative stress, DNA damage, DNA repair and mitochondrial dysfunction in depression. *Progress in Neuro-Psychopharmacology and Biological Psychiatry*, *80*, 309–321. https://doi.org/10.1016/j.pnpbp.2017.06.036

Figures

Fig. 1:

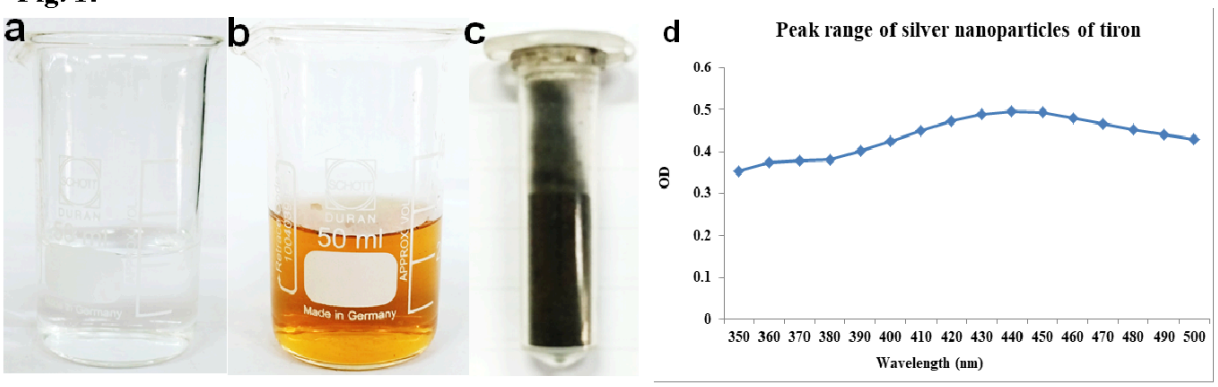

Figure 1

Preparation of nanoparticles: **a** mixture of tiron and silver nitrate solution. **b** Color change as observed after 1 h at 37° C confirmed synthesis of nanoparticles. **c** Dried powder of nanoparticles after scrapping. **d** UV-visible spectroscopic study of tiron-loaded silver nanoparticles

Fig. 2:

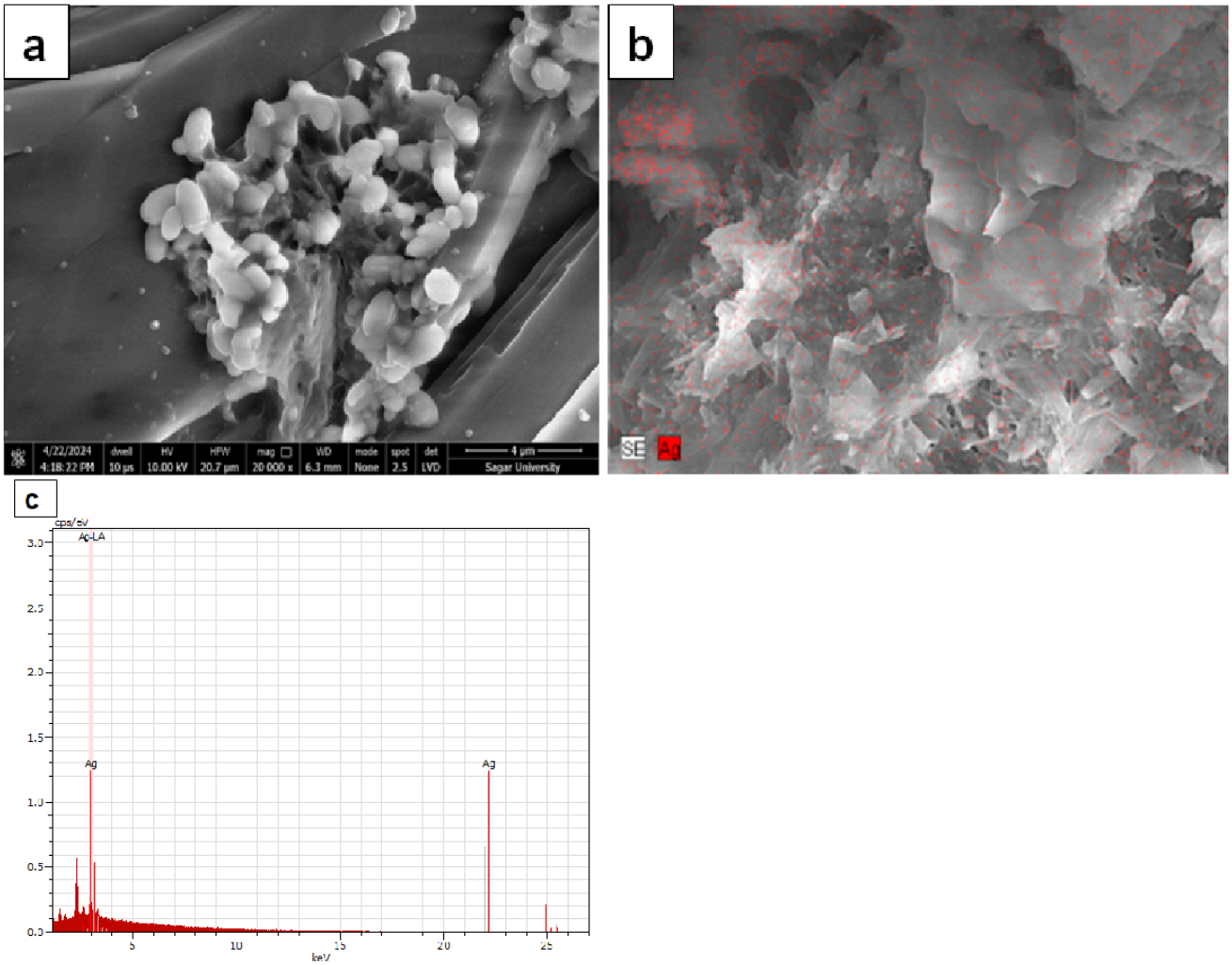

Figure 2

Field emission scanning electron microscopy (SEM) with energy dispersive X-ray (EDX): **a** SEM images of tiron loaded silver nanoparticles showing spherical shapes at 4µm scale. **b** Silver (represented in red dots) distribution over the sample. **c** EDX analysis of tiron loaded silver nanoparticles shows sharp peak at 2.60 keV (Energy).

Fig. 3:

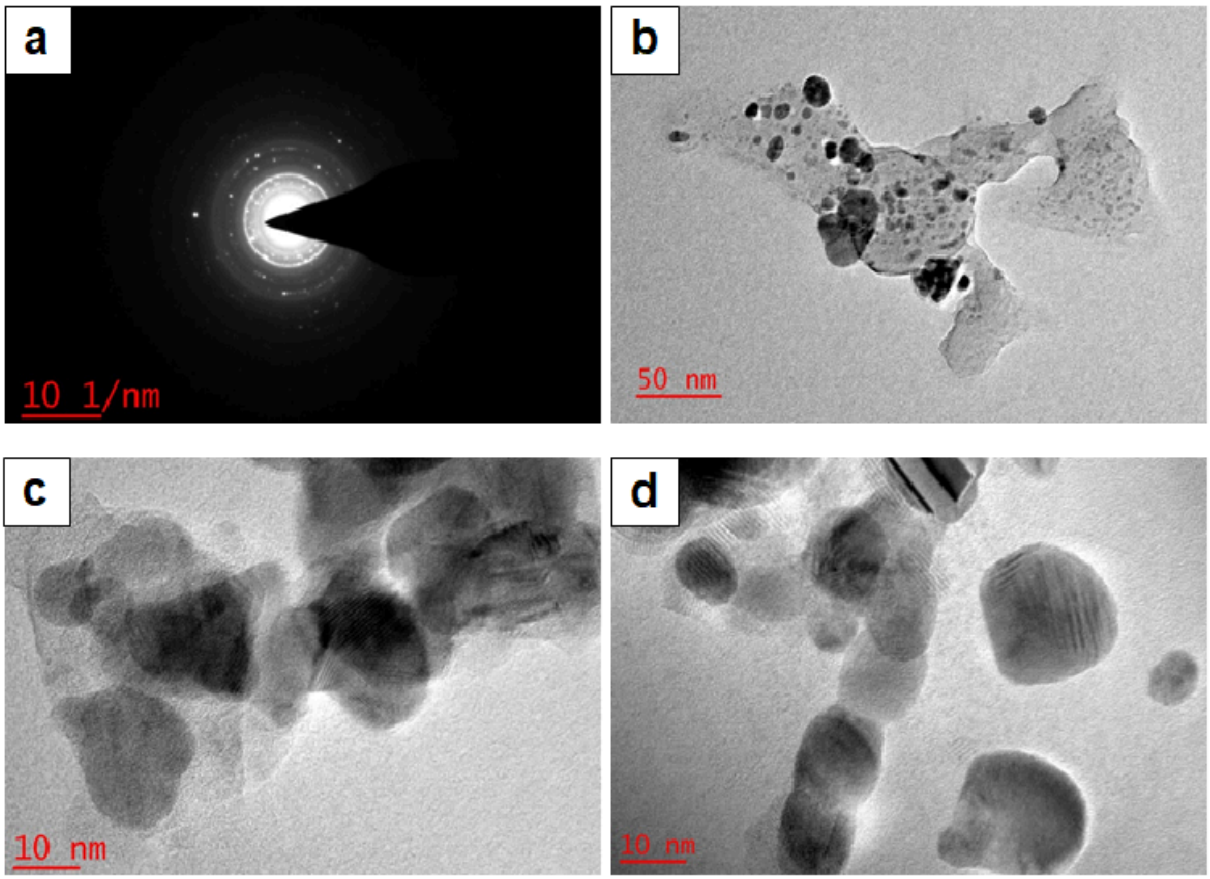

Figure 3

Transmission electron microscopy of tiron loaded silver nanoparticles: **a** HR-TEM image of selected area electron diffraction (SAED) pattern of tiron loaded silver nanoparticles confirmed its polycrystalline and face centered cubic structure. **b** Biosynthesized silver nanoparticles. **c-d** High resolution polycrystalline lattice image of tiron-loaded silver nanoparticles

Fig. 4:

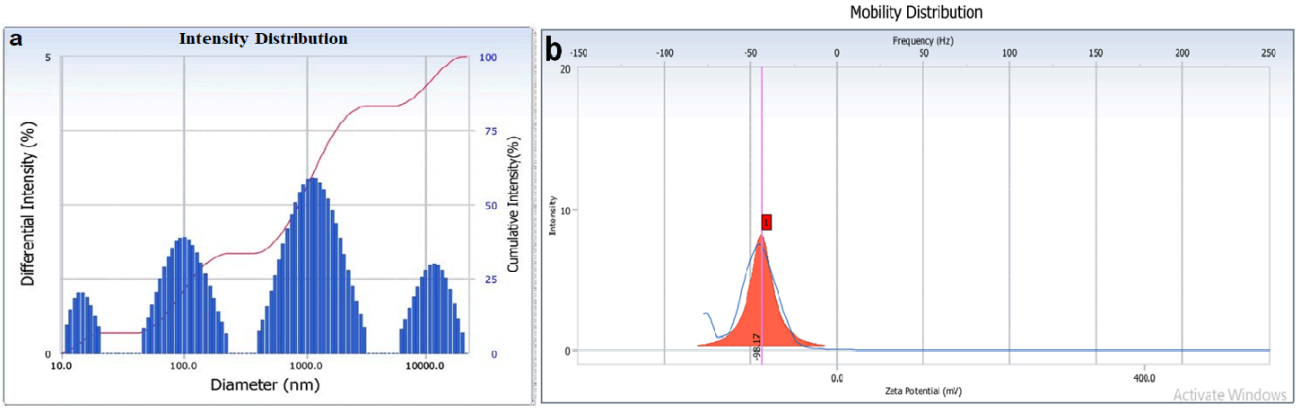

Figure 4

a Particle size distribution (DLS) of tiron loaded silver nanoparticles. **b** Zeta potential analysis of tiron loaded silver nanoparticles

Fig. 5:

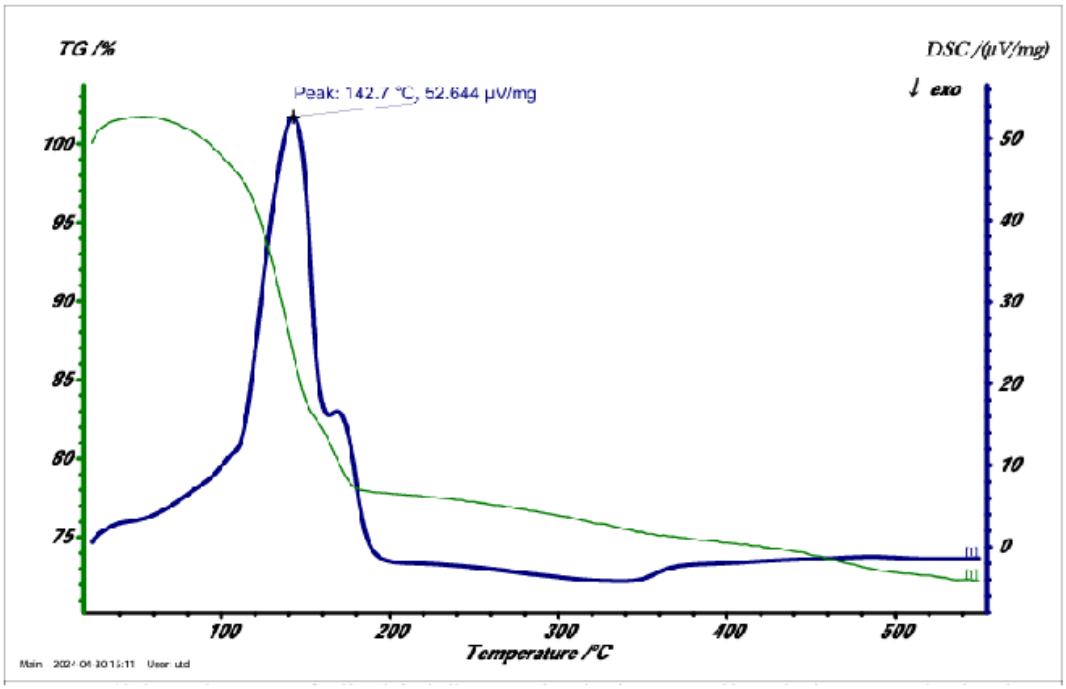

Figure 5

Thermogravimetric analysis of tiron-loaded silver nanoparticles.

Fig. 6:

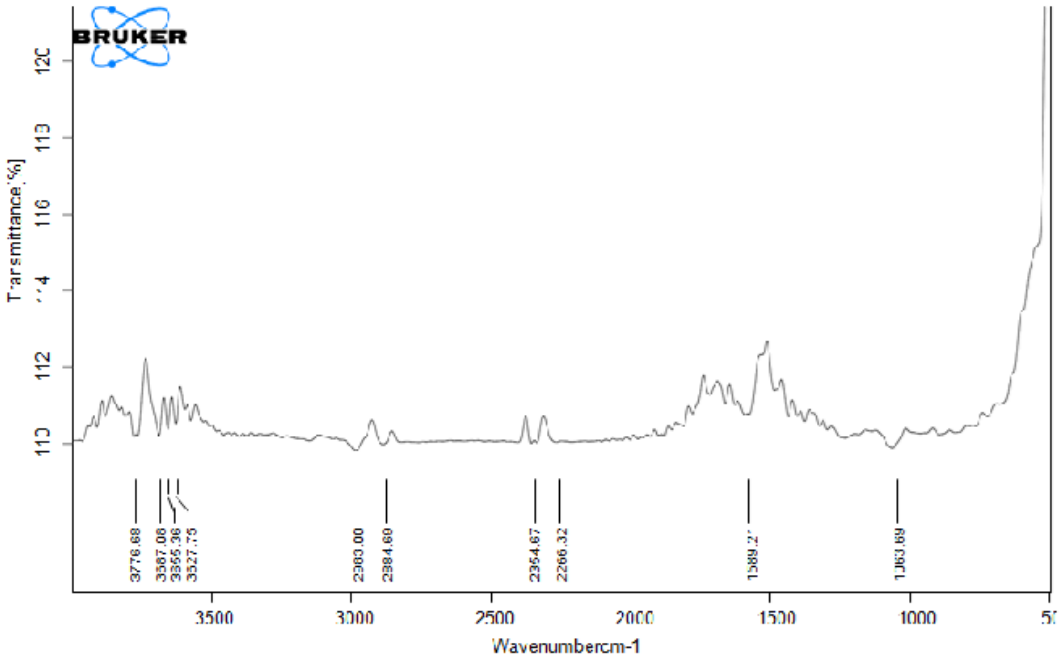

Figure 6

The FTIR of tiron-loaded silver nanoparticles

Fig. 7:

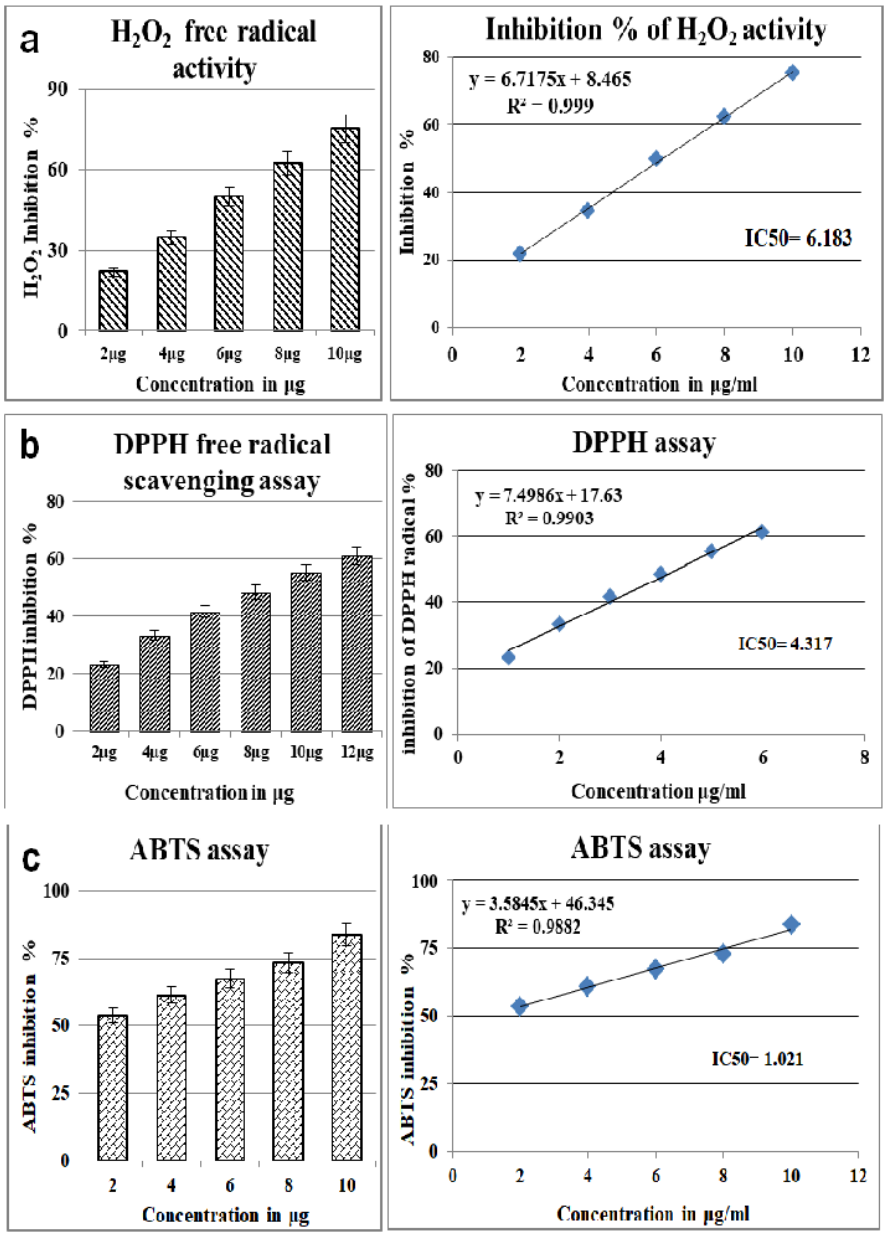

Figure 7

a H_2O_2 scavenging activity of tiron-loaded silver nanoparticles. Data are presented at mean ±SE. **b** DPPH free radical scavenging activity of tiron-loaded silver nanoparticles. Data are presented at mean ±SE. **c** ABTS activity of tiron-loaded silver nanoparticles. Data are presented at mean ±SE

Fig. 8:

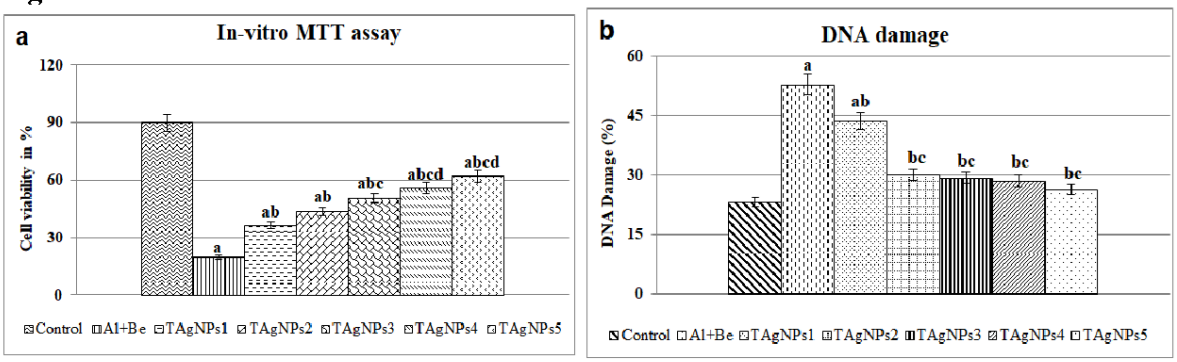

Data are presented at mean ± SE, *control vs Al+Be at $P \leq 0.05$, TAgNPs + (Al+Be) for tukey's HSD post hoc test at $P \leq 0.05$; Significant at 5% level for ANOVA. Abbreviation: Al+Be (aluminium+beryllium) at 1 µg + 6.5 µg, TAgNPs= Tiron loaded silver nanoparticles at 1-5 mg; [a]Control vs Al+Be, TAgNPs 1-5 mg/kg, [b]Al+Be vs TAgNPs 1-5 mg/kg, [c]TAgNPs 1 mg/kg vs TAgNPs 2-5 mg/kg, [d]TAgNPs 2 mg/kg vs TAgNPs 3-5 mg/kg, [e]TAgNPs 3 mg/kg vs TAgNPs 4-5 mg/kg, [f]TAgNPs 4 mg/kg vs TAgNPs 5 mg/kg; **a** In-vitro MTT assay with ANOVA (F-value): 62.83. **b** Genotoxicity assay measured as DNA damage with ANOVA (F-value): 36.98.

Figure 8

a *In-vitro* MTT assay showing cell viability. **b** DNA damage percentage of lymphocytes

Fig. 9:

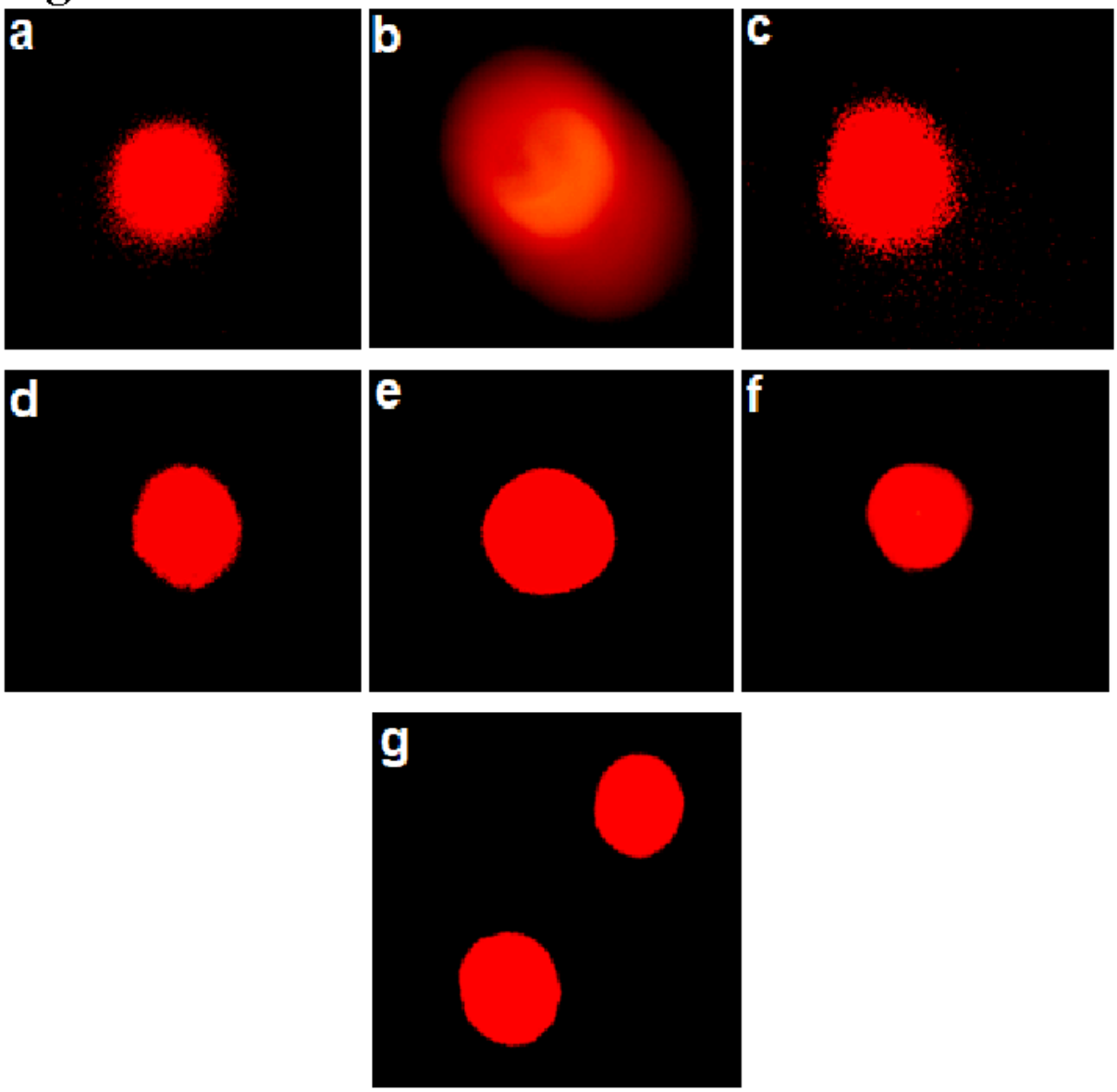

Figure 9

DNA damage detected by comet assay and therapeutic potential of tiron-loaded silver nanoparticles. **a** Control, **b** Toxicant, **c**toxicant+TAgNPs 1 mg, **d**toxicant+TAgNPs 2 mg, **e**toxicant+TAgNPs 3 mg, **f**toxicant+TAgNPs 4 mg, **g** toxicant+TAgNPs 5 mg